Available online at www.sciencedirect.com
SCIENCE DIRECT
Journal of Catalysis 233 (2005) 297–307
JOURNAL OF CATALYSIS
www.elsevier.com/locate/jcat

In situ investigations of structure–activity relationships of a Cu/ZrO_2 catalyst for the steam reforming of methanol

A. Szizybalski [a], F. Girgsdies [a], A. Rabis [b], Y. Wang [c], M. Niederberger [c], T. Ressler [a,*]

[a] *Department of Inorganic Chemistry, Fritz-Haber-Institut of the Max-Planck-Society, Faradayweg 4-6, 14195 Berlin, Germany*
[b] *Department of Solid-State Physics, Max Planck Institute for Chemical Physics of Solids, Nöthnitzer Strasse 40, 01178 Dresden, Germany*
[c] *Colloid Department, Max Planck Institute of Colloids and Interfaces, Research Campus Golm, 14424 Potsdam, Germany*

Received 7 January 2005; revised 18 April 2005; accepted 21 April 2005

Available online 6 June 2005

Abstract

Structure–activity relationships of a nanostructured Cu/ZrO_2 catalyst for the steam reforming of methanol (MSR) were investigated under reaction conditions by in situ X-ray absorption spectroscopy (XAS) and X-ray diffraction (XRD) combined with on-line mass spectrometry (MS). Temperature-programmed activation by reduction in hydrogen or by reduction in a mixture of methanol and water (feed) was studied by time-resolved Cu K edge XANES and TG/DSC/MS measurements. Small and disordered CuO particles were identified as the main copper phase present in the precursors. After extended time on stream and treatment at 673 K in hydrogen, no significant sintering of the copper particles or deactivation of the reduced Cu/ZrO_2 catalysts was detected, indicating a superior stability of the material. The initially low steam-reforming activity of the Cu/ZrO_2 catalyst after reduction in hydrogen could be significantly increased by a temporary addition of oxygen to the feed. This increased activity after oxidative treatment is correlated with an increasing amount of oxygen in the copper particles. ^{63}Cu NMR studies detected only a minor degree of microstrain in the active copper phase of the Cu/ZrO_2 catalyst. The decreased reducibility of CuO/ZrO_2, the low degree of microstrain, and the correlation between the amount of oxygen remaining in the copper particles and the catalytic activity indicate a different metal support interaction compared with Cu/ZnO catalysts.

Keywords: Methanol steam reforming; Copper; Zirconia; XAS; XRD; TG/DSC; Structure–activity correlations; In situ

1. Introduction

Hydrogen fuel cells are promising candidates for the generation of electrical power for mobile applications. Instead of handling H_2 under high-pressure or cryogenic conditions, steam reforming of methanol (MSR) can be used to produce hydrogen on board [1,2]. Improvements in the long-term stability, the hydrogen production rate, and the selectivity of suitable MSR catalysts are subjects of current research in heterogeneous catalysis. Recently, we presented a binary Cu/ZrO_2 catalyst that is more active compared with a commercial $Cu/ZnO/Al_2O_3$ catalyst and more stable during time on stream and produces less CO [3]. However, detailed structure–activity relationships of the Cu/ZrO_2 material are still lacking and are the subject of this work.

Copper-based materials have been extensively studied under MSR and methanol synthesis reaction conditions. However, the structure of the active phase in the catalysts and corresponding structure–activity relationships are still under debate. It has been suggested that the activity of Cu/ZnO-based catalysts is influenced by the morphology and the structural disorder of the copper particles, or by the incorporation of copper into ZnO [4–7]. We have previously reported that the activity of Cu/ZnO catalysts for the methanol synthesis reaction and the methanol steam reforming correlate with the microstrain in the copper phase [8,9]. The strain in the copper nanoparticles originates at the Cu–ZnO interface and emphasizes the role of ZnO in the microstructure of the active copper phase in addition to the prevention

* Corresponding author. Fax: +49 30 8413 4405.
E-mail address: ressler@fhi-berlin.mpg.de (T. Ressler).

0021-9517/$ – see front matter
doi:10.1016/j.jcat.2005.04.024

of sintering. For the MSR reaction we could also show that the increase in activity after a temporary addition of oxygen to methanol and water is correlated with an increase in the disorder in the copper particles [10]. In addition to structure–activity relationships, the stability of copper catalysts and the production of carbon monoxide are important issues with respect to the use of methanol as a source for hydrogen for fuel-cell applications. $Cu/ZnO/Al_2O_3$ catalysts have been shown to deactivate considerably during extended times on stream and treatment at elevated temperatures, which may not be acceptable for the application in mobile fuel-cell applications [11].

In addition to conventional Cu/ZnO-based catalysts, Lindström et al. [1] compared copper-based catalysts (where oxides of Cu, Zn, Cr, and Zr were impregnated on alumina pellets) in the MSR reaction and found that a Cu/ZrO_2 catalyst exhibited the highest selectivity for CO_2. Breen and Ross [12] reported on coprecipitated Cu/ZrO_2 catalysts showing high turnover frequencies, comparable to those of Cu/ZnO catalysts at 498 K. They found that the copper surface area and, hence, the dispersion and the activity were lower compared with Cu/ZnO catalysts. Cu/ZrO_2 catalysts (with $\sim$ 2% Cu) were also reported to produce more methanol from a CO/H_2 mixture per copper surface area than a $Cu/ZnO/Al_2O_3$ catalyst ($>$ 10% Cu) [13]. Nitta et al. [14] found that Cu/ZrO_2 is more active in methanol synthesis than Cu/ZnO at higher temperatures ($>$ 473 K) and that ZrO_2 results in an increased methanol selectivity and diminishes the production of CO.

Here we report studies of a nanostructured Cu/ZrO_2 catalyst for methanol steam reforming prepared by simultaneous precipitation of zirconium dioxide and copper oxide. The complementary bulk techniques of in situ X-ray diffraction (XRD) and X-ray absorption spectroscopy (XAS) were used to elucidate correlations between activity, stability, and structural changes of the Cu/ZrO_2 catalyst under MSR reaction conditions.

2. Experimental

2.1. Preparation of the Cu/ZrO_2 catalyst

The Cu/ZrO_2 nanopowder was synthesized via a precipitation method [15]. Zirconium propylate (11.15 mmol, 5 ml, 70 wt% in 1-propanol; Aldrich) was added to an aqueous solution of tetramethylammonium hydroxide (TMAOH) (2.5 mmol) that we prepared by mixing 1.05 ml TMAOH (25% in methanol) with 43 ml distilled water. After 1 h of stirring, 2.2 ml of a 0.5 M copper nitrate solution was added. The amounts of Cu and Zr were adjusted to yield a catalyst with 10 mol% Cu and 90 mol% Zr. The resulting white suspension was stirred at room temperature for 1 h and finally heated at 353 K for 20 h. After centrifugation and washing, the sample was calcined at 773 K under air for 12 h (ramp 2 K/min). X-ray fluorescence analysis (Seiko SEA 2010) revealed a copper concentration of 8.9 mol% in the calcined CuO/ZrO_2 catalyst precursor.

2.2. X-ray diffraction

Ex situ X-ray diffraction (XRD) measurements were performed on a STOE theta/theta diffractometer (Cu-K_α radiation, secondary monochromator, scintillation counter) in reflection geometry. In situ XRD measurements were conducted on a STOE Bragg–Brentano diffractometer (secondary Si monochromator, scintillation counter) equipped with a Bühler HDK S1 high-temperature chamber [16]. For the in situ experiments, 30 mg of catalyst was dispersed onto a steel ribbon. The gases (He, O_2, H_2) and MeOH and H_2O were introduced into the chamber, as described in more detail in Ref. [10]. The composition of the gas phase was monitored with a quadrupole mass spectrometer (QMS 200; Pfeiffer).

The Cu/ZrO_2 catalyst was reduced in 2 vol% H_2 in He with a total flow of 100 ml/min (heating rate of 6 K/min). At 523 K the sample was held for about 2 h. During this time XRD patterns were recorded in a 2θ range from 25° to 65°, with a counting rate of 3 s/step and a step width of 0.04° 2θ. For studies under MSR reaction conditions, helium was used as a carrier gas and saturated with methanol or water at 293 K and atmospheric pressure (volume ratio of methanol/water = 2:1 (3 vol%:1.5 vol%) (methanol (p_{MeOH} = 12496.1 Pa, 1.13 ml/min) and water (p_{H_2O} = 2337.8 Pa, 0.57 ml/min)); 8 ml/min He flow for MeOH and 24 ml/min He flow for H_2O). After the reduction in hydrogen and cooling to room temperature the gases were changed to MSR conditions, and the sample was again heated to 523 K at a rate of 6 K/min. Crystallite size calculations were based on the Scherrer equation [17]. The K_{α_2} contribution was removed from the pattern with the help of the software package STOE WinXPOW 1.06. Subsequently, we determined the full width at half-maximum (FWHM) by fitting a pseudo-Voigt profile function to the Cu (111) and the ZrO_2 (111) peak.

2.3. X-ray absorption spectroscopy (XAS)

XAS investigations at the Cu K edge (E = 8.979 keV) were performed at beamlines X1 and E4 at HASYLAB at DESY (Hamburg, Germany). Sixty-eight milligrams of the calcined CuO/ZrO_2 precursor was mixed with 200 mg of polyethylene and pressed with a force of 1 ton into a pellet 13 mm in diameter. A copper reference foil was used for energy calibration. The energy range was limited to 8900–9500 eV because of the Hf L_3 edge at 9561 eV (Hf is a natural impurity in zirconium compounds). In situ XAS investigations of the catalyst under reaction conditions were also performed at the Cu K edge in the transmission mode. Ten milligrams of the catalyst ($\sim$ 200 μm grain size), together with 30 mg of boron nitride (BN), was pressed with a force of 1 ton (500 MPa) into a pellet 5 mm in diameter. The

total flow through the in situ cell [18] was set at 40 ml/min at a cell volume of 4 ml, resulting in a methanol conversion of about 6.9%. Two different activation procedures were applied. In the first procedure the catalyst was heated with 6 K/min to 523 K in 2 vol% H_2/He until no further changes in the XANES spectra could be observed. The in situ cell was rapidly cooled to room temperature, and an EXAFS spectrum was measured for detailed structural analysis. Subsequently, the feed of water and methanol for the steam-reforming reaction (methanol/water = 2:1; see above for detailed concentrations) was introduced into the reactor, and the catalyst was heated to 523 K at 6 K/min. In order to reveal the effect of a temporary oxidative treatment [3,5], after 5 h on stream 10 vol% O_2 was added to the feed for about 30 min.

In the second procedure the catalyst was reduced in a mixture of methanol and water (ratio 2:1; see above) at 523 K at a heating rate of 6 K/min. Because the catalyst was already active after this treatment, 10 vol% O_2 was temporarily added to the feed after 1 h. Subsequently, the catalyst was treated at 673 K in 2 vol% H_2/He for 30 min in order to test the stability of the material at elevated temperatures. After cooling to 523 K the gas atmosphere was changed back to MSR conditions, followed by the addition of oxygen and continued methanol steam reforming.

Analysis of the XAFS spectra was performed with the software WinXAS 3.1 [19]. The spectra were energy calibrated with respect to the Cu K edge position of a copper reference foil. After background correction, normalization, and transformation into the k-space, an atomic background $\mu_0(k)$ was determined, with the use of a cubic spline function. The radial distribution function $FT(\chi(k)k^3)$ was obtained by Fourier transformation of the k^3-weighted experimental $\chi(k)$ function ($k = 2.3$–10 Å^{-1}), multiplied by a Bessel window, into the R space. Theoretical backscattering phases and amplitudes were calculated with FEFF 7 [20]. Refinements with the standard EXAFS equation were carried out in R space, with the use of the Cu–Cu coordination shells for copper metal and, when necessary, the first Cu–O shell of Cu_2O. One E_0 shift and one 3rd cumulant for all scattering paths, the Debye–Waller factors (DWF) for the single scattering paths, and the single shell distances were determined by a least-squares fit to the experimental data. Coordination numbers and S_0^2 (0.9) were kept invariant.

For the quantification of the contribution of Cu–O scatterers to the EXAFS $FT(\chi(k)k^3)$, we performed a refinement of the experimental spectra as described above, taking copper metal (first Cu–Cu shell at $R = 2.56$ Å) and the first Cu–O shell of Cu_2O ($R = 1.84$ Å) into account and varying the ratio of the two phases. The DWF of the Cu–O distance was set at 0.0037 Å^2 and kept invariant. This value was determined by a refinement to an experimental spectrum of bulk Cu_2O and, therefore, is based on the static and dynamic disorder of bulk Cu_2O.

A principal component analysis (PCA) of the experimental XANES spectra recorded during the reduction of the catalyst was performed to obtain the number and type of chemical phases present [21]. For the nanostructured catalyst studied here, XAFS spectra of common references like Cu foil or CuO were not able to sufficiently describe the experimental spectra (e.g., small and disordered copper phases). However, to describe the evolution of the phase composition during reduction, the "abstract concentrations" resulting from the PC analysis are compared. The evolution of the "abstract concentrations" corresponds to the evolution of the primary components in the material during reduction. Their absolute values, however, do not represent the real concentration of these components.

2.4. N_2O decomposition

N_2O decomposition was used to determine the copper surface area after activation in methanol and water and after temporary oxygen addition at 523 K. N_2O decomposition (reactive frontal chromatography, RFC) was first introduced by Chinchen et al. [22] and can be readily applied to copper catalysts in situ after various treatment steps in a conventional quartz reactor. In the work reported here, the following procedure was used. After activation in the feed (second procedure in the XAS section) the sample was purged for 1 h in He at 523 K with a flow of 50 ml/min to diminish the amount of adsorbed molecules. Afterward, the sample was cooled to 313 K. N_2O decomposition was performed at 313 K with a mixture of 0.5 vol% N_2O/He at a flow of 15 ml/min, with the sample placed on a quartz frit in a quartz tube reactor. The sample was diluted with boron nitride to provide a bed height of about 15 mm, with a thermocouple positioned in the powder bed.

In contrast to the original RFC method described by Chinchen et al., we chose to monitor the amount of $m/e = 44$ (representing N_2O) consumed during the "reactive frontal chromatography." For a blank measurement, the reactor was filled with an appropriate amount of boron nitride. N_2O/He was passed through the sample bed, and the evolution of the MS ion currents of N_2O ($m/e = 44$), N_2 ($m/e = 28$), and He ($m/e = 4$) was monitored. For measurements of the catalyst, detection of the $m/e = 44$ current (N_2O) occurs later compared with the boron nitride blank experiment, because N_2O reacts with the surface of the copper particles to yield nitrogen. To calculate the Cu surface area, the inflection points of the N_2O ion current traces ($m/e = 44$) from the N_2O decomposition measurements were determined as the endpoint of the titration. Subsequently, the areas under the N_2O ion current traces of the catalyst (A) and the blank measurement (B) were calculated, and the difference between the areas A and B was used to calculate the corresponding volume of N_2 produced by the decomposition of N_2O. We calculated the copper surface area, assuming 1.47×10^{19} copper atoms per square meter [22]. In addition to measuring Cu/ZrO_2 samples, we performed N_2O decomposition on Cu/ZnO samples, where the copper surface areas have previously been presented [4]. Comparable results were obtained

with the procedure used here. From repeated measurements of the material under the same reaction conditions, the experimental error was estimated to be about 15%.

2.5. TG-DSC/MS

The TG-DSC measurements were performed on a Netzsch STA 449C. The evolution of the gas-phase composition was monitored with an Omnistar mass spectrometer (Pfeiffer). About 26 mg of the catalyst material was put in an Al_2O_3 crucible and positioned on the TG/DSC sample holder. An empty Al_2O_3 crucible was used for the reference.

2.6. Nuclear magnetic resonance spectroscopy

For nuclear magnetic resonance (NMR) investigations, various samples were collected from a fixed-bed reactor after various reaction steps and transferred into NMR tubes in a glove box without exposure to air. Cu NMR spectra of the Cu/ZrO_2 catalysts were measured with a Bruker MSL 300 spectrometer at 79.618 MHz for ^{63}Cu and at 85.288 MHz for ^{65}Cu at 4.2 K in an Oxford cryostat. Spin-echo experiments (90°-τ-180°) were performed with a 90° pulse of 5.5 µs, a "recycling delay" of 2 s, and a tau value of 25 µs. The ^{63}Cu-NMR spectra shown were calibrated against $CuBr_{(s)}$ at −381 ppm.

3. Results

3.1. XRD investigation of the precursor and the reduced Cu/ZrO_2 catalyst

The XRD pattern of the calcined CuO/ZrO_2 shows tetragonal ZrO_2 as the major crystalline phase (Fig. 1a), with a minor contribution of monoclinic ZrO_2 (5–8%). The pattern exhibits no peaks corresponding to a copper oxide phase. Measurements with Al_2O_3 as an internal standard yielded a good crystallinity of the sample (> 95%). The crystallite size of the tetragonal ZrO_2 is about 70 Å, as calculated on the basis of the FWHM of the ZrO_2 (111) peak. After the reduction of the precursor material (inset in Fig. 1b) in 2 vol% H_2/He, a small Cu (111) peak is observed (copper crystallite size ∼ 20 Å). Exposure to the steam-reforming feed or oxygen addition cycles has no significant influence on the diffraction patterns of Cu or CuO and the zirconia phases.

3.2. Local structure of the CuO/ZrO_2 precursor

Fig. 2a shows Cu K-edge XANES spectra for the CuO/ZrO_2 precursor material and the CuO reference (obtained by calcination of malachite) measured at room temperature. Compared with the spectrum of CuO, the characteristic pre-edge at 8984 eV and the peaks after the absorption edge are less pronounced in the spectrum of the CuO/ZrO_2 precursor. The differences in the $FT(\chi(k)k^3)$ of the catalyst precursor and the CuO reference are clearly visible in Fig. 3. Instead of one peak representing the second nearest oxygen and copper neighbors in CuO (at distances of 2.8 and 2.9 Å), the $FT(\chi(k)k^3)$ of the CuO/ZrO_2 precursor exhibits two strongly reduced peaks at ∼ 3.0 Å. Nevertheless, a theoretical XAFS function of a CuO model structure could be successfully refined to the experimental spectrum of the CuO/ZrO_2 precursor, resulting in good agreement between theory and experiment in the range from 1.0 to 4.0 Å in the $FT(\chi(k)k^3)$ (Fig. 3). This indicates that disordered CuO is the main copper phase present in the CuO/ZrO_2 precursors.

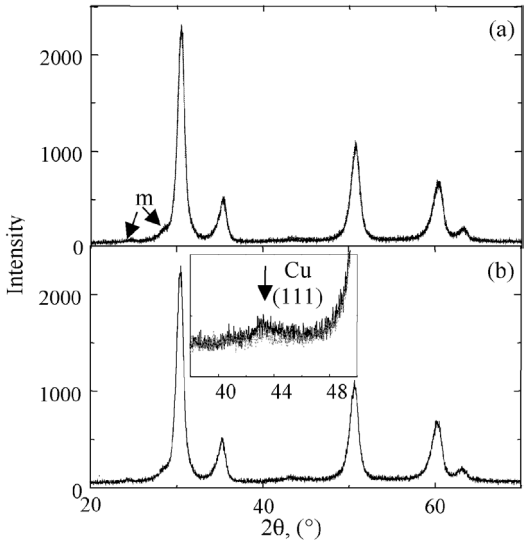

Fig. 1. XRD patterns of (a) CuO/ZrO_2 precursor and (b) after reduction in 2 vol% H_2/He. Arrows indicate small peaks of monoclinic zirconia (m) and copper metal.

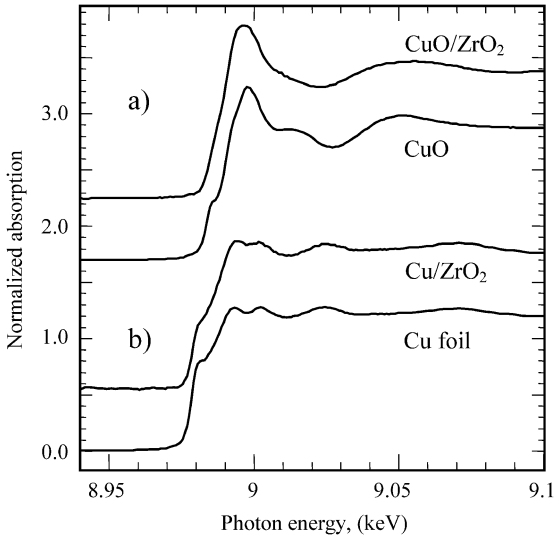

Fig. 2. Cu K-edge XANES spectra of (a) CuO/ZrO_2 precursor together with CuO, (b) Cu/ZrO_2 after reduction in 2 vol% H_2/He at 523 K together with Cu metal.

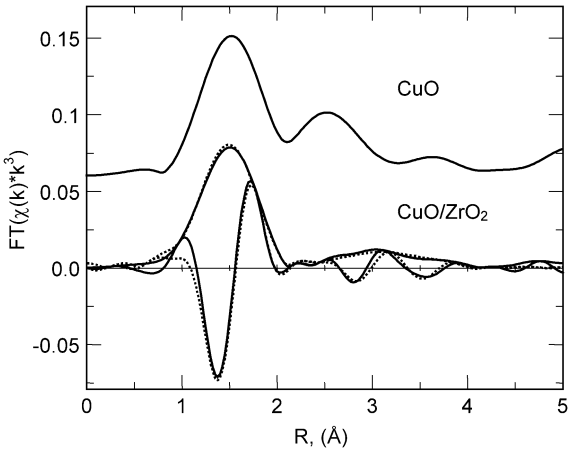

Fig. 3. Refinement of a theoretical Cu K edge $FT(\chi(k)k^3)$ (dotted line) of CuO to the experimental $FT(\chi(k)k^3)$ of the CuO/ZrO_2 precursor (solid line) together with the experimental $FT(\chi(k)k^3)$ of a CuO reference.

Table 1
Specific copper surface areas calculated on basis of N_2O decomposition measurements or crystallite sizes from in situ XRD investigation and hydrogen production rates (industrial $Cu/ZnO/Al_2O_3$ catalyst, $S_{Cu} = 32.4\ m^2/g_{Cu}$, $R_{H_2} = 33.2\ \mu mol/(g_{Cu}\ s)$, $TOF = 4.8\ min^{-1}$)

Treatment	S_{Cu} (m^2/g_{Cu}) [N_2O]	H_2 production rate (μmol/(g_{Cu} s))	TOF (min^{-1})	S_{Cu} (m^2/g_{Cu}) [XRD]
After reduction in feed at 523 K	13.2	44.0	82	9.2
After first addition of O_2 after reduction in feed	10.4	48.0	113	11.5
After high temperature treatment in hydrogen	15.7	42.3	67	6.7
After second addition of O_2 after high temperature treatment in hydrogen	30.7	47.0	41	10.6

3.3. N_2O decomposition

The specific copper surface area was determined by N_2O decomposition (A) after reduction of the CuO/ZrO_2 material in a quartz glas tube reactor in methanol and water, (B) after temporary addition of oxygen to the feed, (C) after treatment at 673 K in hydrogen, and (D) after a second addition of oxygen to the feed. Although the first oxygen addition yielded a slight decrease in Cu surface area of the Cu/ZrO_2 catalyst, the resulting Cu surface exhibited a higher activity in the steam reforming of methanol. The corresponding turnover frequencies (TOFs) were calculated on the basis of the specific copper surface area S_{Cu} (m^2/g_{Cu}) and the corresponding hydrogen production rate (μmol/(s g_{Cu})) (Table 1). The hydrogen production rate and the specific copper surface are were determined after ∼ 30 min time on stream, when the activity of the Cu/ZrO_2 catalyst had reached a constant level. Whereas the MSR activity exhibited a constant increase after the first addition of oxygen, a spiked increased followed by deactivation was observed after the high-temperature treatment and the second addition of oxygen. Based on the crystallite size (XRD) and assuming spherical particles, the volume ($\rho_{Cu} = 8.92\ g/cm^3$) of all copper particles and the corresponding surface area were also determined. Except for the copper surface area after treatment at 673 K and oxygen addition to the feed, the surface areas based on the XRD crystallite size compare well with those obtained by N_2O decomposition (Table 1). For comparison, the catalytic performance and the copper surface area of an industrial $Cu/Al_2O_3/ZnO$ catalyst with about 50 wt% copper were determined under identical conditions. Although this catalyst possesses a higher surface area (32.4 m^2/g_{Cu}) than the Cu/ZrO_2 catalyst (13.2 m^2/g_{Cu}), it exhibits an inferior TOF (Table 1).

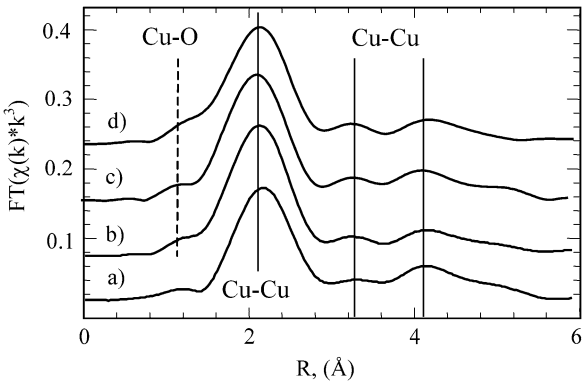

Fig. 4. $FT(\chi(k)k^3)$ of (a) copper metal, (b) Cu/ZrO_2 after reduction in 2 vol% H_2/He at 523 K, (c) Cu/ZrO_2 after reduction in 2 vol% H_2 followed by MSR, and (d) Cu/ZrO_2 after reduction in methanol and water (feed).

3.4. Reduction of CuO/ZrO_2 in 2% H_2/He

The normalized XANES spectrum of the catalyst at 523 K after reduction in hydrogen is plotted in Fig. 2b, together with that of a reduced copper reference at 523 K (commercial CuO; Merck). The reduced Cu/ZrO_2 catalyst shows edge features similar to that of Cu metal obtained from the reduction of CuO. The characteristic doublet in the post-edge region (8.99–9.0 keV) is also well resolved. The $FT(\chi(k)k^3)$ of the Cu/ZrO_2 catalyst (Fig. 4b) strongly resembles that of the copper reference (Fig. 4a). Only slight differences can be seen in the shape of the peaks and in the small shoulder visible on the left of the first Cu–Cu shell in the $FT(\chi(k)k^3)$ of the Cu/ZrO_2 catalyst. Fig. 5 shows the result of a XAFS refinement of a copper model structure with an additional Cu–O distance ($R = 1.84$ Å, ∼ 21%) to the experimental $FT(\chi(k)k^3)$ of the Cu/ZrO_2 catalyst after reduction in 2% H_2 at 523 K. With the addition of an oxygen nearest neighbor it was possible to simulate the first peak in the $FT(\chi(k)k^3)$, whereas the contribution from higher shells of copper oxide phases were not detectable in the remaining spectrum. In order to corroborate the validity of our approach to analyzing the experimental Cu K edge XAFS data of the Cu/ZrO_2 catalyst under reaction conditions, Fig. 6 shows a simulated $FT(\chi(k)k^3)$ for a mixture of 20% Cu–O in Cu_2O and 80% Cu metal at 523 K, together

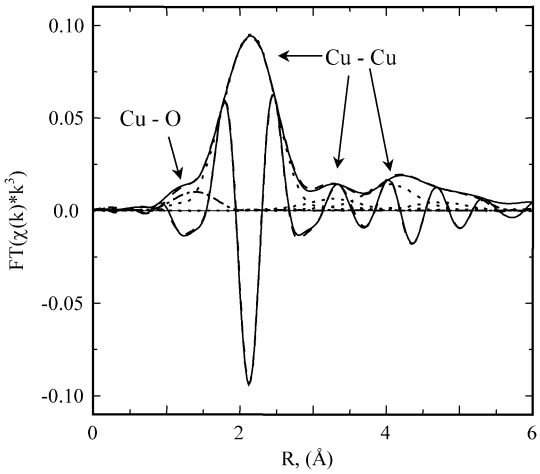

Fig. 5. Refinement of a theoretical Cu K edge $FT(\chi(k)k^3)$ (dotted line) of copper metal and one additional Cu–O distance to the experimental $FT(\chi(k)k^3)$ of the Cu/ZrO_2 catalyst after reduction in 2 vol% H_2 at 523 K (solid line).

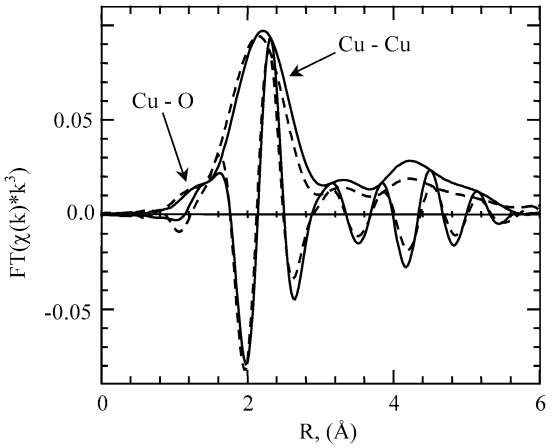

Fig. 6. Simulated $FT(\chi(k)k^3)$ (solid) for a mixture of 20% Cu_2O and 80% Cu in comparison with the experimental $FT(\chi(k)k^3)$ (dashed) of the Cu/ZrO_2 catalyst after reduction in methanol and water at 523 K.

with an experimental $FT(\chi(k)k^3)$ of the catalyst after reduction in 2 vol% H_2/He. The amplitude of the oxygen shoulder and the imaginary part are well reproduced by the simulation.

3.5. Reduction kinetics

A PC analysis of time-resolved XANES spectra of CuO/ZrO_2 measured during reduction in 2 vol% H_2 yielded three primary components sufficient to reconstruct the experimental data. The evolution of the abstract concentrations during the reduction in 2 vol% H_2/He indicates a third component as an intermediate phase (Fig. 8b), probably corresponding to Cu_2O. Fig. 8a shows that the reduction in hydrogen started at a lower temperature compared with the reduction in methanol and water. Peak reduction temperatures (corresponding to the maximum reduction rate, i.e., the inflection point of the sigmoidal trace) were determined to be 461 and 496 K, respectively.

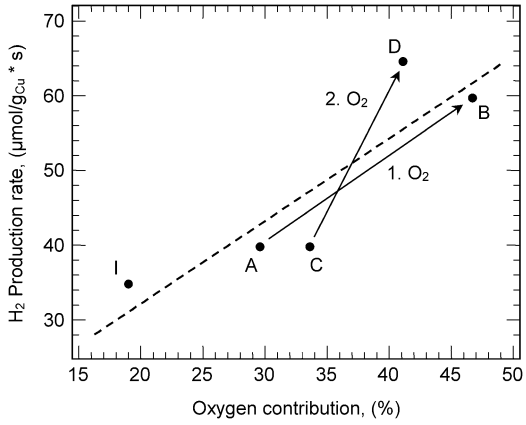

Fig. 7. Oxygen contribution to the Cu K edge $FT(\chi(k)k^3)$ of the Cu/ZrO_2 catalyst (I) after reduction in 2 vol% H_2/He at 523 K followed by switching to feed (methanol and water), (A) after reduction in feed, (B) after first addition of oxygen to the feed, (C) after heating to 673 K in 2 vol% H_2/He and switching to feed, and (D) after second addition of oxygen to the feed together with the corresponding H_2 production rates (not normalized to the specific copper surface area) measured in the XAS in situ cell (Fig. 10). The arrows indicate the increase in oxygen contribution and production rate after first (1. O_2) and second (2. O_2) addition of oxygen.

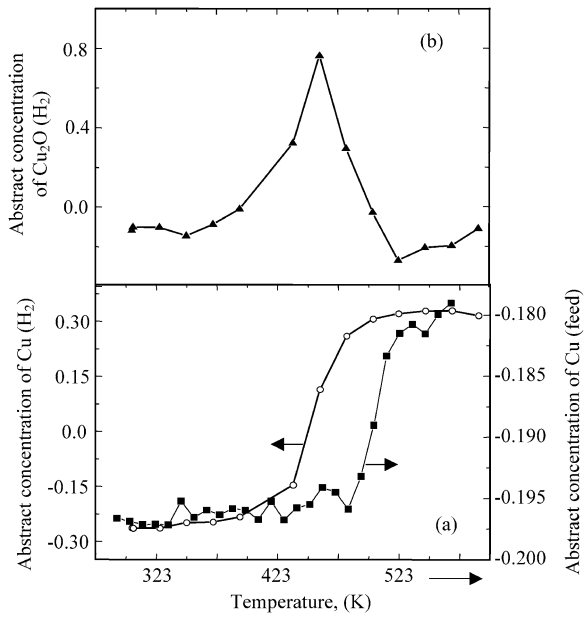

Fig. 8. Evolution of (a) the abstract concentrations (PCA) of Cu during reduction in 2 vol% H_2 and during reduction in methanol and water (feed) and (b) of the abstract concentration of the intermediate CuO_2 phase during reduction in 2 vol% H_2.

Before TG-DSC measurements, the CuO/ZrO_2 sample was heated twice to 523 K in He and held at that temperature for 1 h to remove adsorbed water and CO_2. Subsequently, the catalyst was heated in 2 vol% H_2/He from 300 to 523 K at a heating rate of 6 K/min. Two exothermic DSC signals between 423 and 440 K (Fig. 9a) correlate with two peaks in the MS water signal (Fig. 9b). During reduction the sam-

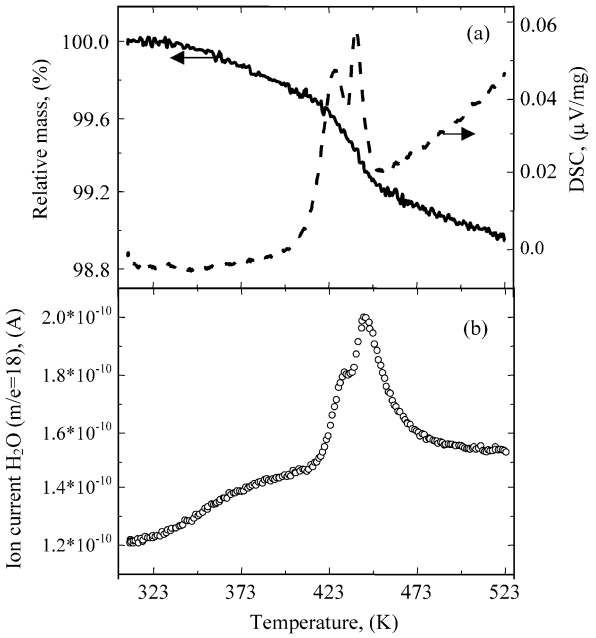

Fig. 9. (a) Evolution of mass loss (solid) and DSC signal (dashed) during reduction of the CuO/ZrO_2 precursor in 2 vol% H_2/He from 300 to 523 K at 6 K/min and (b) evolution of the corresponding MS signal of water ($m/e = 18$).

ple exhibits a weight loss of ∼ 0.9%. This is less than what was calculated for a complete reduction of CuO/ZrO_2 to Cu/ZrO_2 (1.2%) and corroborates the incomplete reduction detected by in situ XAS.

3.6. Steam reforming of methanol

Fig. 4d depicts the $FT(\chi(k)k^3)$ of the Cu/ZrO_2 catalyst reduced in methanol and water. The position and shape of the first peak (i.e., first Cu–Cu shell) are very similar to the peak of the sample reduced in hydrogen (Fig. 4b). The main difference can be seen in the reduced amplitude of the Cu–Cu peak in the $FT(\chi(k)k^3)$ and the increased height of the Cu–O shoulder. After reduction in 2 vol% H_2 the Cu/ZrO_2 catalyst exhibits a low initial activity in the steam reforming of methanol (Fig. 7). After reduction in the feed, however, the Cu/ZrO_2 catalyst possesses a significantly increased activity in the MSR. The $FT(\chi(k)k^3)$ of the catalyst reduced in the feed exhibits a Cu–O peak with a higher amplitude (∼ 30%) (Fig. 4, c and d) compared with that of the catalyst reduced in hydrogen (∼ 20%) (Fig. 7).

After reduction of the Cu/ZrO_2 catalyst in the feed at 523 K, the temperature was kept constant until no further changes were observed in the XAFS spectra. The temporary addition of oxygen and partial re-reduction in the feed resulted in a considerably increased activity of the Cu/ZrO_2 catalyst (Fig. 10). The Cu K edge $FT(\chi(k)k^3)$, measured after various reaction steps, is depicted in Fig. 11. Significant differences are observable in the amplitude of the Cu–O shoulder and the first Cu–Cu peak. The corresponding oxygen contribution to the $FT(\chi(k)k^3)$ is depicted in Fig. 7;

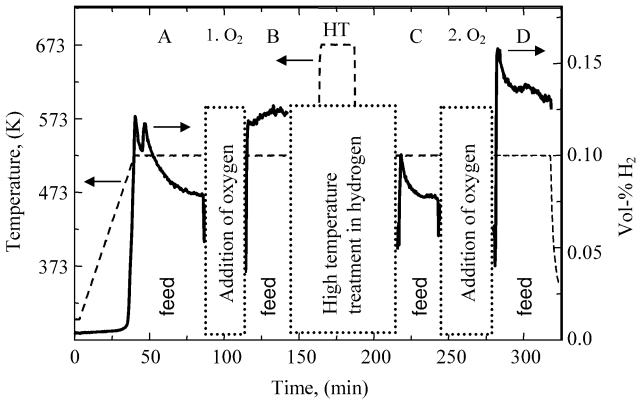

Fig. 10. Evolution of H_2 production rate during methanol steam reforming on a Cu/ZrO_2 catalyst measured in the in situ XAS cell during and after various treatments: (A) reduction in methanol and water at 523 K (feed), (1. O_2) first temporary addition of oxygen (10 vol% O_2) to the feed, (B) feed after first addition of oxygen, (HT) treatment in 2 vol% H_2 at 673 K, (C) feed after treatment at 673 K, (2. O_2) second addition of oxygen to the feed, (D) feed after second addition of oxygen.

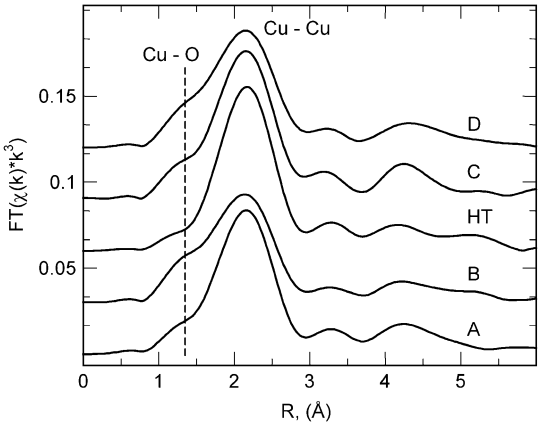

Fig. 11. Cu K edge $FT(\chi(k)k^3)$ of the Cu/ZrO_2 catalyst measured in situ after various treatments (Fig. 10): (A) reduction in methanol and water at 523 K (feed), (B) feed after first temporary addition of oxygen (10 vol% O_2), (HT) treatment in 2 vol% H_2 at 673 K, (C) feed after treatment at 673 K, (D) feed after second addition of oxygen.

this indicates that an increasing amount of oxygen remains in the copper particles after oxidation and re-reduction. Fig. 7 shows that after the first and second additions of oxygen, the increase in hydrogen production rate of the Cu/ZrO_2 catalyst (Fig. 10) correlates with an increasing amount of oxygen.

3.7. High-temperature treatment of Cu/ZrO_2 in H_2

After MSR and the addition of oxygen, the Cu/ZrO_2 catalyst was heated in 2 vol% H_2/He to 673 K. After the catalyst was cooled to 523 K in hydrogen, a XAFS analysis of the experimental Cu K edge $FT(\chi(k)k^3)$ revealed complete reduction of the copper phase to copper metal clusters on ZrO_2. The only slightly increased amplitude of the first Cu–Cu peak in the $FT(\chi(k)k^3)$ excludes major sintering of the Cu particles during the high-temperature treatment in hydrogen. Subsequent steam reforming of methanol resulted in

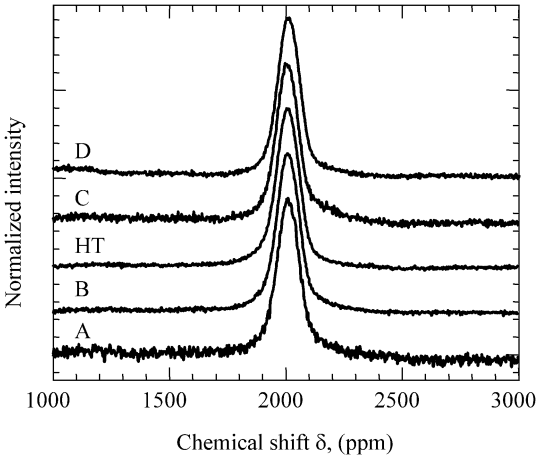

Fig. 12. ^{63}Cu NMR spectra of the Cu/ZrO_2 catalyst measured ex situ after various treatments: (A) reduction in methanol and water at 523 K (feed), (B) feed after first temporary addition of oxygen (10 vol% O_2), (HT) treatment in 2 vol% H_2 at 673 K, (C) feed after treatment at 673 K, (D) feed after second addition of oxygen.

similar activities, as after initial reduction of the catalyst in the feed (Fig. 10). The XAFS $FT(\chi(k)k^3)$ measured under MSR reaction conditions after hydrogen treatment exhibits again a pronounced contribution of an oxygen nearest neighbor. Moreover, adding oxygen to the feed (Fig. 10) resulted in a strong increase in activity and an increase in the amount of oxygen in the copper particles (Figs. 7 and 11). The corresponding TOFs (based on the specific copper surface area per gram of copper) of the various reaction steps as determined in a quartz reactor are given in Table 1. It can also be seen from Table 1 that the copper surface area as determined by N_2O decomposition increased considerably after hydrogen treatment at 673 K and addition of oxygen to the feed.

A copper crystallite size of ~ 20 Å was determined from the Cu (111) XRD line, exhibiting only small changes after the various reaction steps. Changes in the copper crystallite size should also be detectable in the Debye–Waller factors of the first Cu–Cu shell [23]. However, for the nanostructured Cu/ZrO_2 catalysts described here, the additional Cu–O shell and the limited data range render a reliable determination of crystallite size effects from an EXAFS analysis difficult.

3.8. Nuclear magnetic resonance spectroscopy

Similar to X-ray diffraction line broadening, a symmetric and narrow ^{63}Cu NMR line profile indicates large and ordered crystallites. Hence, a decrease in the copper crystallite size results in a symmetric NMR line broadening, whereas an increase in strain or disorder causes an asymmetric NMR line profile [9,24]. Fig. 12 shows ^{63}Cu NMR spectra for the Cu/ZrO_2 catalyst after various reaction steps. In addition to differences in the amplitude, it can be seen that the width of the NMR lines varies only slightly as a function of the treatment conditions.

4. Discussion

4.1. Structure of the CuO/ZrO_2 precursor

Small CuO particles and low concentration of Cu in the material (8%) account for the fact that no copper oxide phases are detected in the XRD pattern of the CuO/ZrO_2 precursor (Fig. 1). XAFS measurements of the precursor material identified CuO as the main copper phase (Figs. 2 and 3). The deviations between the $FT(\chi(k)k^3)$ of the reference CuO and the CuO/ZrO_2 precursor in the amplitude of the higher shells (Fig. 3) are caused by a strongly disordered structure and/or small crystallite sizes of the nanostructured CuO/ZrO_2 precursor [3]. Okamoto et al. proposed highly dispersed Cu^{2+} in CuO/ZrO_2 to account for the deviations from ideal CuO in the $FT(\chi(k))$ [25]. However, a calcination temperature of 973 K used by these authors may have resulted in a considerable incorporation of Cu in ZrO_2, which renders a comparison with the Cu/ZrO_2 material prepared here difficult.

Zhou et al. have reported on Cu/ZrO_2 catalysts, consisting mostly of tetragonal zirconia for copper concentrations less than 10 wt% [26]. They suggested an interaction between copper oxide and the ZrO_2 support that prevents phase transformation to monoclinic ZrO_2 according to the oxygen vacancy model of Sanchez and Gazquez [27]. Various metal centers in ZrO_2 (e.g., Y, Ce, Al, Cu) were reported to stabilize tetragonal zirconia [28–30]. Because no incorporation of Cu into the ZrO_2 lattice was detectable by XRD or EXAFS (complete reduction of Cu at 673 K, detection limit ~ 1%), a significant stabilizing effect of Cu centers in ZrO_2 can be excluded for the nanostructured Cu/ZrO_2 catalysts [3]. Garvie et al. [31,32] and Chraska et al. [33] discussed the influence of the particle size on the stability of the tetragonal phase and found that for small particles ($r_{\text{critical}} \approx 9$–30 nm) the stability of the tetragonal phase at room temperature can be explained by the lower surface energy of t-ZrO_2 compared with m-ZrO_2. This may explain the stabilization of the tetragonal ZrO_2 particles with a diameter of about 7 nm in addition to the influence of the copper phase and the particular preparation technique on the surface termination of the ZrO_2 particles

4.2. Reduction of the CuO/ZrO_2 precursor

Two DSC signals at 423 and 440 K measured during reduction of the CuO/ZrO_2 precursor correspond to the reduction of CuO to Cu_2O and Cu_2O to Cu metal, respectively, with Cu_2O as an intermediate of the reduction (Fig. 9). The PC analysis of the in situ XAFS spectra also shows that the reduction in 2 vol% H_2/He and methanol/water proceeds via an intermediate phase (Fig. 8a). Hence, a bimodal particle size distribution like that suggested for Cu on Y-doped ZrO_2 [34] with small CuO clusters and bulk CuO that reduce at ~ 423 and ~ 448 K, respectively, should not be the

main source for the DSC/MS signals measured. The formation of an intermediate Cu_2O phase during the reduction of CuO/ZrO_2 in both hydrogen and methanol/water (feed) is in agreement with our previous results for Cu/ZnO catalysts. The reduction temperatures determined by the PC analysis indicate that the reduction of CuO/ZrO_2 in the feed is shifted to higher temperatures, probably because of the oxidizing influence of water and carbon dioxide [10,35] (Fig. 8). The increased reduction temperature, however, does not seem to result in significantly larger Cu particles. In contrast to the reduction of Cu/ZnO under similar conditions, the reduction of the CuO/ZrO_2 precursor in 2 vol% H_2/He at 523 K did not result in pure copper metal clusters on ZrO_2, but in a partially oxidized copper phase (Figs. 5 and 7).

4.3. Structure of the activated Cu/ZrO_2 catalyst

In contrast to Cu/ZnO catalysts that appear to be completely reduced at 523 K in 2% H_2, the activated Cu/ZrO_2 catalyst exhibits a lower degree of reduction with a considerable amount of oxygen still detectable in the Cu K-edge XAFS data (Figs. 4 and 7). High-temperature treatment of the Cu/ZrO_2 catalyst in hydrogen resulted in a complete reduction of the copper oxide phase to copper metal (Fig. 11). Hence, the remaining amount of oxygen detectable after initial reduction in methanol and water or after re-reduction following the addition of oxygen to the feed cannot be ascribed to isolated copper centers in the ZrO_2 or copper oxide particles inaccessible to the gas phase. From the XAFS data for the Cu/ZrO_2 catalyst shown here, it is difficult to distinguish between oxygen in the copper particles, a mixture of separated Cu clusters and very small Cu oxide particles, or a copper oxide interface between the Cu clusters and the ZrO_2 support. Because the experimental $FT(\chi(k)k^3)$ of activated Cu/ZrO_2 catalysts can be well described beyond the first shell by Cu metal alone (Fig. 5), a considerable amount of large or well-crystallized Cu_2O particles can be excluded. Additionally, no isolated copper oxide particles were detected in TEM measurements on a Cu/ZrO_2 sample prepared and activated in a manner similar to what is described here. This seems to corroborate the presence of either oxygen in the copper particles or a copper oxide interface layer.

4.4. High-temperature treatment of Cu/ZrO_2 in H_2

During reduction in H_2 at 673 K, the Cu/ZrO_2 catalyst exhibited only minor sintering of the Cu particles (Table 1, Figs. 11 and 12). Conversely, Cu/ZnO catalysts treated at 673 K in hydrogen exhibit strong sintering, accompanied by loss of copper surface area and catalytic activity. This process appears to be irreversible for Cu/ZnO materials, whereas the fully reduced Cu/ZrO_2 catalyst can be re-activated by an oxidation/re-reduction treatment. Hence, the Cu/ZrO_2 catalyst described here possesses a considerable stability toward temporarily increasing temperatures, which may make it more suitable for use in mobile applications under changing reaction conditions.

4.5. Methanol steam reforming on a Cu/ZrO_2 catalyst

A linear correlation between the specific copper surface area and methanol synthesis activity has already been proposed by Chinchen et al. [4]. However, additional factors influence the activity of copper catalysts, and deviations in the microstructure of the catalysts may result in differently active copper surfaces. Similar to our results for Cu/ZnO catalysts [8–10], the MSR activity of the Cu/ZrO_2 catalyst described here (Table 1) exhibits no simple linear correlation with the specific Cu surface area. A sufficient copper surface area is a prerequisite for an active methanol catalyst; however, it cannot account for the differences observed after the various oxidation/reduction treatments (Table 1). Whereas after the first addition of oxygen to the MSR feed the detectable Cu surface area decreased, the corresponding H_2 production rate increased, indicating a more active specific copper surface (i.e., higher TOF). Conversely, after high temperature reduction and addition of oxygen to the feed, the Cu surface area increased considerably, accompanied by a constant H_2 production rate. This corresponds to a less active specific Cu surface (i.e., a lower TOF) after the second addition of oxygen, possibly because of a deteriorated interaction between the Cu metal and ZrO_2 support. It seems that also in the Cu/ZrO_2 systems, additional microstructural parameters must be considered to account for the differently active specific Cu surfaces observed.

In contrast to our previous reports for the correlation of microstrain and activity of Cu/ZnO catalysts [8,9], ^{63}Cu NMR spectroscopy studies of differently treated Cu/ZrO_2 catalysts yielded nearly symmetric NMR lines (Fig. 12) regardless of the treatment conditions. This is indicative of only minor amounts of microstrain in the copper phase in the Cu/ZrO_2 materials. Moreover, it seems that the varying amount of oxygen in the copper phase dependent on the treatment conditions has very little effect on the degree of strain detectable in the copper particles. The characteristic epitaxial relationship between Cu and ZnO in the conventional Cu/ZnO catalysts is the most likely origin of the microstrain in the copper phase of these materials. Apparently, Cu on ZrO_2 exhibits a different metal support interaction, which does not result in detectable strain in the copper particles.

After reduction in hydrogen, the Cu/ZrO_2 catalyst exhibited little initial catalytic activity. However, under methanol steam-reforming conditions, temporarily adding oxygen to the feed before or after the high-temperature reduction resulted in an increased catalytic activity (Figs. 7 and 10) accompanied by an increased amount of oxygen in the copper particles (Figs. 4 and 7). Similarly, addition of oxygen results in an increase in copper crystallite size of Cu/ZnO catalysts and, thus, a decrease in the specific copper surface area [10]. After the addition of oxygen, the Cu/ZnO catalysts

re-reduced completely in the feed, and an increased catalytic activity was obtained that correlated with an increased degree of microstrain in the copper particles. In contrast to Cu/ZnO, the increased amount of oxygen remaining in the copper particles of Cu/ZrO_2 after oxygen addition to the feed is indicative of an incomplete re-reduction. A comparable correlation between activity and oxidation of copper has been reported for Cu/Al_2O_3 and Cu/ZnO catalysts, suggesting a partial re-oxidation of copper metal to Cu_2O after a certain activation time in the MSR feed [36]. Cheng et al. [28] correlated the MSR activity of copper on an oxygen ion conducting yttria–ceria–alumina support with the availability of oxygen adsorption sites and, hence, enhanced oxidation of Cu to Cu^+. For the catalyst investigated here such an interaction is not evident; nevertheless it is possible that oxygen stored at the surface of the ZrO_2 support stabilizes partially oxidized copper clusters or a copper oxide interface layer.

The lower reducibility of Cu/ZrO_2 and the small degree of microstrain in the copper particles strongly suggest a different metal support interaction between Cu and ZrO_2 compared with Cu and ZnO. Apparently, the defective microstructure of the Cu/ZrO_2 catalyst under reaction conditions considerably influences the catalytic activity and results in differently active specific copper surfaces, depending on the treatment conditions. For the nanostructured Cu/ZrO_2 catalyst studied here it is proposed that the incomplete re-reduction after the temporary addition of oxygen to the feed increases the effect of the oxidized copper bulk structure on the electronic structure of copper sites at the surface. Hence, the increase in reactivity observed after the addition of oxygen may be correlated with a change in the filling of the copper d-band and, thus, changes in adsorption or dissociation energies. A comparable influence on the electronic Cu surface structure is ascribed to the microstrain in Cu/ZnO catalysts, indicating that the two effects may be complementary in modifying the catalytic activity of copper in methanol chemistry.

5. Summary

In situ bulk structural investigations of a nanostructured Cu/ZrO_2 catalyst under methanol steam-reforming conditions were performed to reveal structure–activity relationships. Small and disordered CuO particles were identified as the main copper phase present in the precursors. The initial low steam-reforming activity of the Cu/ZrO_2 catalyst after reduction in hydrogen could be significantly increased by a short addition of oxygen to the feed. Reduction of the Cu/ZrO_2 catalyst in the feed or re-reduction after oxidation resulted in supported nanoparticles with an increased amount of oxygen in the copper particles, which correlates with the increased activity of the Cu/ZrO_2 catalyst. In contrast to conventional Cu/ZnO catalysts, only a minor degree of microstrain is detected in the active copper phase of Cu/ZrO_2 catalysts. The decreased reducibility of CuO/ZrO_2, the low degree of microstrain, and the correlation between the amount of oxygen remaining in the copper particles and catalytic activity indicate a different metal support interaction compared with Cu/ZnO catalysts. Similar to Cu/ZnO catalysts, however, the interaction between Cu and ZrO_2 stabilizes an active copper microstructure that strongly deviates from that of bulk copper metal.

Acknowledgments

The authors are grateful to the ZEIT Foundation, Hamburg, Germany, and the German Research Foundation, DFG (SPP 1091 “Brückenschläge in der heterogenen Katalyse”) for financial support. The Hamburger Synchrotronstrahlungslabor, HASYLAB, is acknowledged for providing beamtime for this work. We thank R.E. Jentoft and B.L. Kniep for participating in the XAS measurements. R. Schlögl is acknowledged for his continuous support.

References

[1] B. Lindström, L.J. Pettersson, Int. J. Hydrogen Energy 26 (2001) 923.
[2] P.J. de Wild, M.J.F.M. Verhaak, Catal. Today 60 (2000) 3.
[3] H. Purnama, F. Girgsdies, T. Ressler, J.-H. Schattka, R.A. Caruso, R. Schomäcker, R. Schlögl, Catal. Lett. 94 (2004) 61.
[4] G.C. Chinchen, K.C. Waugh, D.A. Whan, Appl. Catal. 25 (1986) 101.
[5] P.L. Hansen, J.B. Wagner, S. Helveg, J.R. Rostrup-Nielsen, B.S. Clausen, H. Topsøe, Science 295 (2002) 2053.
[6] J.B. Bulko, R.G. Herman, K. Klier, G.W. Simmons, J. Phys. Chem. 83 (1979) 3118.
[7] B.S. Clausen, J. Schiøtz, L. Gråbæk, C.V. Ovesen, K.W. Jacobsen, J.K. Nørskov, H. Topsøe, Top. Catal. 1 (1994) 367.
[8] M.M. Günter, T. Ressler, B. Bems, C. Buscher, T. Genger, O. Hinrichsen, M. Muhler, R. Schlögl, Catal. Lett. 71 (2001) 37.
[9] B.L. Kniep, T. Ressler, A. Rabis, F. Girgsdies, M. Baenitz, F. Steglich, R. Schlögl, Angew. Chem. 116 (2004) 114.
[10] M.M. Günter, T. Ressler, R.E. Jentoft, B. Bems, J. Catal. 203 (2001) 133.
[11] M. Kurtz, H. Wilmer, T. Genger, O. Hinrichsen, M. Muhler, Catal. Lett. 86 (2003) 77.
[12] J.P. Breen, J.R.H. Ross, Catal. Today 51 (1999) 521.
[13] B. Denise, R.P.A. Sneeeden, Appl. Catal. 30 (1987) 353.
[14] Y. Nitta, O. Suwata, Y. Ikeda, Y. Okamoto, T. Imanaka, Catal. Lett. 26 (1994) 345.
[15] Y. Wang, R.A. Caruso, J. Mater. Chem. 12 (2002) 1442.
[16] T. Ressler, R.E. Jentoft, J. Wienold, M.M. Günter, O. Timpe, J. Phys. Chem. B 104 (2000) 6360.
[17] H.P. Klug, L.E. Alexander, X-Ray Diffraction Procedures, Wiley, New York, 1945, 491 pp.
[18] Designed by M. Hagelstein, T. Neisius et al., ESRF, France in a collaborative effort with the Fritz-Haber-Institute, Berlin, Germany (see also Ref. [17]).
[19] T. Ressler, J. Synch. Radiat. 5 (1998) 118.
[20] S.I. Zabinsky, J.J. Rehr, A. Ankudinov, R.C. Albers, M.J. Eller, Phys. Rev. B: Condens. Matter 52 (1995) 2995.
[21] T. Ressler, J. Wong, J. Roos, I.L. Smith, Environ. Sci. Technol. 34 (2000) 950.
[22] G.C. Chinchen, C.M. Hay, H.D. Vandervell, K.C. Waugh, J. Catal. 103 (1987) 79.

[23] B.S. Clausen, L. Grabek, H. Topsøe, L.B. Hansen, P. Stoltze, J.K. Norskow, O.H. Nielsen, J. Catal. 141 (1993) 368.
[24] A.V. Chadwick, I.J.F. Poplett, D.T.S. Maitland, M.E. Smith, Chem. Mater. 10 (1998) 864.
[25] Y. Okamoto, H. Gotoh, H. Aritani, T. Tananka, S. Yoshida, J. Chem. Soc., Faraday Trans. 93 (1997) 3879.
[26] R.-X. Zhou, T.-M. Yu, X.-Y. Jiang, F. Chen, X.-M. Zheng, Appl. Surf. Sci. 148 (1999) 263.
[27] M.G. Sanchez, J.L. Gazquez, J. Catal. 104 (1987) 120.
[28] W.-H. Cheng, I. Chen, J.-S. Liou, S.-S. Lin, Top. Catal. 22 (2003) 225.
[29] M.K. Dongare, V. Ramaswamy, C.S. Gopinath, A.V. Ramasamy, S. Scheurell, M. Brueckner, E. Kemnitz, J. Catal. 199 (2001) 209.
[30] M.M. Cervera, M. Escobar, M.C. Caracche, P.C. Rivas, A.M. Rodriguez, Hyperfine Interact. 120/121 (1999) 469.
[31] R.C. Garvie, J. Phys. Chem. 82 (1978) 218.
[32] R.C. Garvie, J. Phys. Chem. 69 (1965) 1238.
[33] T. Chraska, A.H. King, C.C. Berndt, Mater. Sci. Eng. A 286 (2000) 169.
[34] L. Kundakovic, M. Flytzani-Stephanopoulos, Appl. Catal. 171 (1998) 13.
[35] R.O. Idem, N.N. Bakhshi, Indian J. Eng. Chem. Res. 33 (1994) 2065.
[36] K. Klier, V. Chatikavanij, R.G. Herman, G.W. Simmons, J. Catal. 74 (1982) 343.